Energy & Environmental Science

RSC Publishing

PAPER

View Article Online
View Journal | View Issue

Cite this: *Energy Environ. Sci.*, 2013, **6**, 918

Thermoelectric composites of poly(3-hexylthiophene) and carbon nanotubes with a large power factor†

Celine Bounioux,[a] Pablo Díaz-Chao,[b] Mariano Campoy-Quiles,[c] Marisol S. Martín-González,[b] Alejandro R. Goñi,[cd] Rachel Yerushalmi-Rozen[e] and Christian Müller‡*[c]

Received 7th September 2012
Accepted 18th December 2012

DOI: 10.1039/c2ee23406h

www.rsc.org/ees

Composite films of poly(3-hexylthiophene) and single- as well as multi-walled carbon nanotubes are demonstrated to offer a competitive thermoelectric performance. The power factor significantly exceeds values obtained with either constituent alone provided that the conjugated polymer is sufficiently p-doped. The use of single-walled carbon nanotubes consistently results in a higher electrical conductivity with a maximum value above 10^3 S cm^{-1} and thus gives rise to a power factor of 25 ± 6 μW m^{-1} K^{-2} for a filler content of only 8 wt% and a maximum 95 ± 12 μW m^{-1} K^{-2} for 42–81 wt%. Moreover, a carbon nanotube content of 8–10 wt% does not compromise the low bulk thermal conductivity of the polymer matrix, which promises a high figure of merit of at least $ZT > 10^{-2}$ at room-temperature. All samples are cast on plastic substrates, emphasising their suitability for large-area, flexible thermoelectric applications.

Introduction

Thermoelectric power generators are solid-state devices that directly convert heat flow to electricity. Unique advantages are their scalability and ability to function with small heat sources and limited temperature differences.[1] Thin and flexible designs that can cover large areas are particularly suited for waste recovery in industrial settings from chimneys to data centres. On the other hand, a miniature power source would be of great benefit for the myriad of autonomous electronic components such as wireless sensors and identification tags that are envisaged to make up tomorrow's *Internet of Things*. Without doubt, large-area as well as small-scale applications will only become viable if cost-effective and robust materials with good thermoelectric properties can be identified. In this paper we concentrate on organic semiconductors and demonstrate that optimally doped conjugated polymer–carbon nanotube composites can offer a competitive performance.

The thermoelectric performance of a material is conveniently described by the dimensionless figure of merit given by:

$$ZT = S^2\sigma\kappa^{-1}T \quad (1)$$

A good thermoelectric material should possess a large Seebeck coefficient S to provide a high voltage,[2,3] a large electrical conductivity σ to minimise Joule heating and a low thermal conductivity κ to reduce heat losses. Alternatively, if the thermal conductivity is unknown the power factor $S^2\sigma$ can serve as a performance indicator. Currently, the champion material at ambient temperature is bismuth telluride (Bi_2Te_3) with a $ZT_{300K} \sim 1$ ($S^2\sigma \sim 1000$ μW m^{-1} K^{-2}),[4] which, however, is brittle and laborious to process. These drawbacks explain why, so far, only niche applications have been explored such as prohibitively expensive wrist watches that run on body heat or radioisotope thermoelectric generators that power spacecraft.[1]

In order to address this demand for alternative thermoelectric materials, conjugated polymers currently receive renewed attention.[5,6] They readily offer the desired ease of processing from solution, which enables printing on large-area, flexible substrates. An additional advantage is the low thermal conductivity $\kappa \sim 0.1$–0.5 W m^{-1} K^{-1} of polymers. Until recently, only doped polyacetylene displayed a promising thermoelectric performance with a power factor up to $ZT_{300K} \sim 0.4$ ($S^2\sigma \sim 932$ μW m^{-1} K^{-2}) but its poor solubility and notorious instability in air prevent any practical use.[7,8] Instead, more environmentally stable materials such as polyaniline, polypyrrole and polythiophenes were found to suffer from an at least one order of magnitude lower figure of merit.[8,9] However, during the last few years two independent approaches have

[a]*Department of Solar Energy and Environmental Physics, Jacob Blaustein Institute for Desert Research, Ben-Gurion University of the Negev, Sede Boker campus, 84990, Israel*
[b]*Instituto de Microelectrónica de Madrid (IMM-CSIC), Calle de Isaac Newton 8, Tres Cantos, 28760 Madrid, Spain*
[c]*Institut de Ciència de Materials de Barcelona (ICMAB-CSIC), Campus de la UAB, 08193 Bellaterra, Spain. E-mail: christian.muller@chalmers.se*
[d]*Institució Catalana de Recerca i Estudis Avançats (ICREA), Passeig Lluis Companys 23, Barcelona, 08010, Spain*
[e]*Department of Chemical Engineering, The Ilse Katz Institute for Nanoscale Science and Technology, Ben-Gurion University of the Negev, 84105 Beer Sheva, Israel*

† Electronic supplementary information (ESI) available. See DOI: 10.1039/c2ee23406h

‡ Present address: Department of Chemical and Biological Engineering/Polymer Technology, Chalmers University of Technology, 41296 Göteborg, Sweden.

been identified that can vastly improve the thermoelectric properties of one material in particular, *i.e.* poly(3,4-ethylenedioxythiophene) (PEDOT). Bubnova *et al.* elegantly demonstrated that a judiciously optimised p-doping level of electropolymerised PEDOT thin films can lead to a $ZT_{300K} \sim 0.25$ ($S^2\sigma \sim 324$ μW m^{-1} K^{-2}).[10,11] In parallel, See *et al.* and Yu *et al.* prepared composites of PEDOT:poly(styrene sulfonic acid) (PEDOT:PSS) with Te nanorods and carbon nanotubes (CNTs), respectively, which resulted in large power factors of up to $S^2\sigma \sim 71$ μW m^{-1} K^{-2} and 160 μW m^{-1} K^{-2}.[12,13] In particular for the former material a figure of merit $ZT_{300K} \sim 0.1$ could be established. Other recent examples are metal coordination compounds. Although these materials are completely insoluble and of low molecular weight, both p- and n-type behaviour could be observed, the latter with a high $S^2\sigma \sim 67$ μW m^{-1} K^{-2} and $ZT_{300K} \sim 0.1$.[14] However, efforts to achieve equally encouraging results with other conjugated polymers have met with lesser success. For instance, attempts to optimally p-dope poly(3-hexylthiophene) (P3HT) or various poly(2,7-carbazole) derivatives only resulted in up to $S^2\sigma \sim 26$ μW m^{-1} K^{-2} and 19 μW m^{-1} K^{-2}, respectively.[9,15,16] Likewise, attempts to compound CNTs with the conjugated polymer polyaniline gave rise to a similar $S^2\sigma \sim 20$ μW m^{-1} K^{-2} ($ZT_{300K} \sim 0.004$),[17,18] whereas P3HT/CNT composites displayed a disappointingly low $S^2\sigma \sim 0.002$ μW m^{-1} K^{-2}.[19] Recently, He *et al.* obtained somewhat better results with doped P3HT/Bi_2Te_3 composites, which yielded $S^2\sigma \sim 14$ μW m^{-1} K^{-2} compared to reference doped P3HT with $S^2\sigma \sim 4$ μW m^{-1} K^{-2}.[20] Worth mentioning are also reports on thermoelectric composites of CNTs with non-conjugated polymers such as poly(vinyl acetate) (PVA),[21,22] polyvinylidene fluoride (PVDF)[23] and Nafion,[24] all of which tend to suffer from insufficient electrical connectivity of dispersed CNTs due to the insulating polymer matrix.

Here, we show that a combination of the above discussed two approaches, *i.e.* compounding with CNTs followed by optimised p-doping, is a practical avenue that can raise the thermoelectric properties of conjugated polymer-based materials to a competitive level. We elected to work with P3HT, arguably the most widely studied conjugated polymer, which so far displayed a particularly frustrating performance.[8,9,19,20] Moreover, we demonstrate that optimally p-doped P3HT/CNT composite films can be readily prepared on plastic substrates, which is a prerequisite for the realisation of flexible, large-area applications.

Results and discussion

Preparation of P3HT/CNT dispersions

In order to facilitate processing, we used the well-documented ability of P3HT to aid dispersion of CNTs by wrapping around or crystallising on their surface.[25–27] Bernardi *et al.* have proposed a detailed interaction mechanism based on self-assembly that is mediated by π-stacking, which explains the observed affinity between P3HT and CNTs.[28] We used a polymer of medium regioregularity ~90%. Initial trials with regiorandom P3HT as well as highly ~97% regioregular P3HT resulted in less promising electrical properties, likely due to the inability of the former to crystallise and the somewhat reduced solubility of the latter. Initially, carbon nanotubes were crudely dispersed in *ortho*-dichlorobenzene (*o*DCB). Despite sonication, macroscopic aggregates continued to exist, which are clearly visible in the photograph displayed in Fig. 1A. In contrast, gradual addition of regioregular P3HT dissolved in chloroform, followed by mild sonication after each addition step resulted in homogeneous dispersion of CNTs. Interestingly, the colour of P3HT solutions rapidly changes from orange to deep red when added to CNT dispersions (Fig. 1A). This pronounced chromism is typical for P3HT, which displays a strong red-shift in absorbance during solidification.[29] Differential scanning calorimetry (DSC) thermograms corroborate the ability of CNTs to assist crystallisation of P3HT. In particular, we observe an increase in melt crystallisation temperature of P3HT when blended with CNTs, which is characteristic of classical nucleation behaviour (ESI, Fig. S1†).

We prepared composites of P3HT and multi-walled (MW) or single-walled (SW) CNTs. P3HT/MW-CNT composites are easier to disperse in organic solvents *via* the above described procedure. In contrast, P3HT/SW-CNT composites usually yield superior electrical properties but demand more laborious processing, which has been discussed in detail by Bauhofer and Kovacs.[30] In particular, to prepare composites with a high SW-CNT content a much larger amount of solvent had to be used

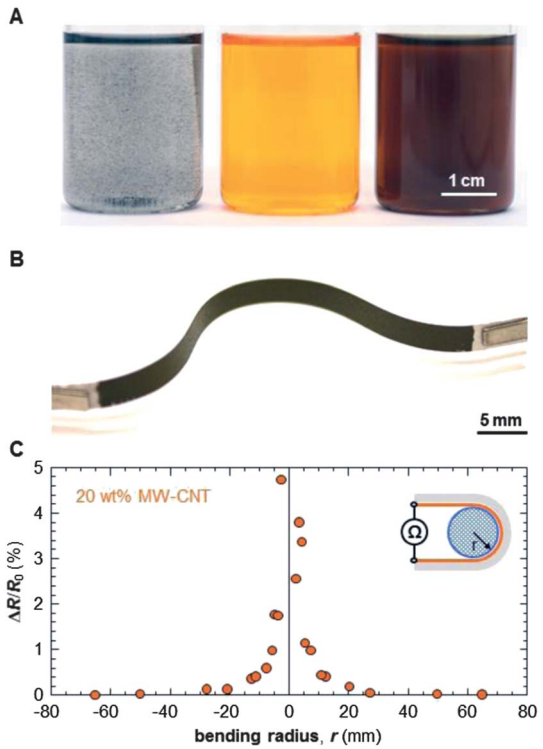

Fig. 1 Processing of P3HT/CNT composites. (A) 5 mg L^{-1} dispersion of MW-CNTs (left); 50 mg L^{-1} solution of P3HT (centre); 50 mg L^{-1} dispersion with $c_{MW\text{-}CNT} \sim 10$ wt% (right). (B) 6 cm long flexible tape composed of a ~2 μm thick composite film with $c_{MW\text{-}CNT} \sim 20$ wt% on PET foil with silver paste contacts on either end. (C) Percentage change in resistance $\Delta R/R_0$ of the curved section of the above tape during bending as a function of bending radius *r*, measured in 2-point configuration. Inset: schematic of the experimental setup used to measure the resistance *R*.

and more vigorous sonication was required. As a result our SW-CNT reference samples displayed significantly lower electrical properties than MW-CNT. Note that we did not use surfactants other than P3HT to disperse CNTs. Despite those limitations, we were able to prepare P3HT/CNT composites across the whole composition range, with a MW-CNT content $c_{\text{MW-CNT}} \sim 2$–50 wt % and a SW-CNT $c_{\text{SW-CNT}} \sim 1$–81 wt%, as well as pure P3HT and CNT reference samples.

Mechanical flexibility of composite films

Micrometre-thick films were prepared by casting P3HT/CNT dispersions on flexible poly(ethylene terephthalate) (PET) substrates, which after drying of the P3HT/CNT film were cut to shape to manufacture final samples. A representative flexible tape is shown in Fig. 1B. In order to investigate to which degree such tapes can be reversibly deformed we monitored the electrical resistance during bending (Fig. 1C). A tape was wrapped 180 degrees around circular objects with decreasing radius (*cf.* inset Fig. 1C), both in convex and concave conformation with respect to the tape surface. We found that up to a bending radius of only 5 mm, the resistance reversibly varied by less than one percent, which dramatically eased sample handling constraints and demonstrates the potential of P3HT/CNT composites for flexible applications.

Thermoelectric properties of undoped composites

With the aim to explore the thermoelectrical properties of the prepared P3HT/CNT composites, in a first set of experiments we characterised the electrical conductivity and Seebeck coefficient of selected samples as a function of temperature. We only observed a weak linear variation between 40 and 105 °C (ESI, Fig. S2†). Thus, we restricted the characterisation to room-temperature measurements of the electrical conductivity and used a home-built setup to estimate an average Seebeck coefficient over a temperature range of 30–100 °C (*cf.* Experimental).

The electrical conductivity of polymer/carbon nanotube composites is sensitive to percolation of the filler material.[31] Reference P3HT displayed a low $\sigma_{\text{P3HT}} \sim 1.7 \pm 0.1 \times 10^{-5}$ S cm^{-1} but addition of CNTs rapidly led to a substantial increase in electrical conductivity (Fig. 2A). Evidently, the highly elongated shape of CNTs permits efficient percolation at low weight fractions. Furthermore, the higher aspect-ratio SW-CNTs percolate at a much lower fraction than MW-CNTs and lead to a significantly higher electrical conductivity overall. We used an empirical relation to fit our data:

$$\sigma = \sigma_{\text{CNT}}|c - c^*|^p \quad (2)$$

where c is the CNT concentration and c^*, σ_{CNT} and p are constants.[32] c^* is the critical CNT concentration for percolation. We obtain best fits with $c_{\text{MW-CNT}}^* \sim 4$ wt% and $c_{\text{SW-CNT}}^* \sim 0.2$ wt%. The pre-factor σ_{CNT} is related to the intrinsic electrical conductivity of CNTs as well as the electrical contact resistance. For P3HT/MW-CNT composites we deduce a value of $\sigma_{\text{MW-CNT}} \sim$ 24 S cm^{-1} in contrast to P3HT/SW-CNT composites that yield a significantly higher $\sigma_{\text{SW-CNT}} \sim 275$ S cm^{-1}. Whereas the electrical conductivity of reference MW-CNT agrees with this estimate, pristine SW-CNT films perform poorly, *i.e.* the measured electrical conductivity is much lower than the theoretically obtained value $\sigma_{\text{SW-CNT}}$. This, we rationalise with the difficulty to process SW-CNTs without the aid of a suitable dispersing agent such as P3HT. The power law exponent p describes the dimensionality of the system and has a value of $p_{2D} = 4/3$ and

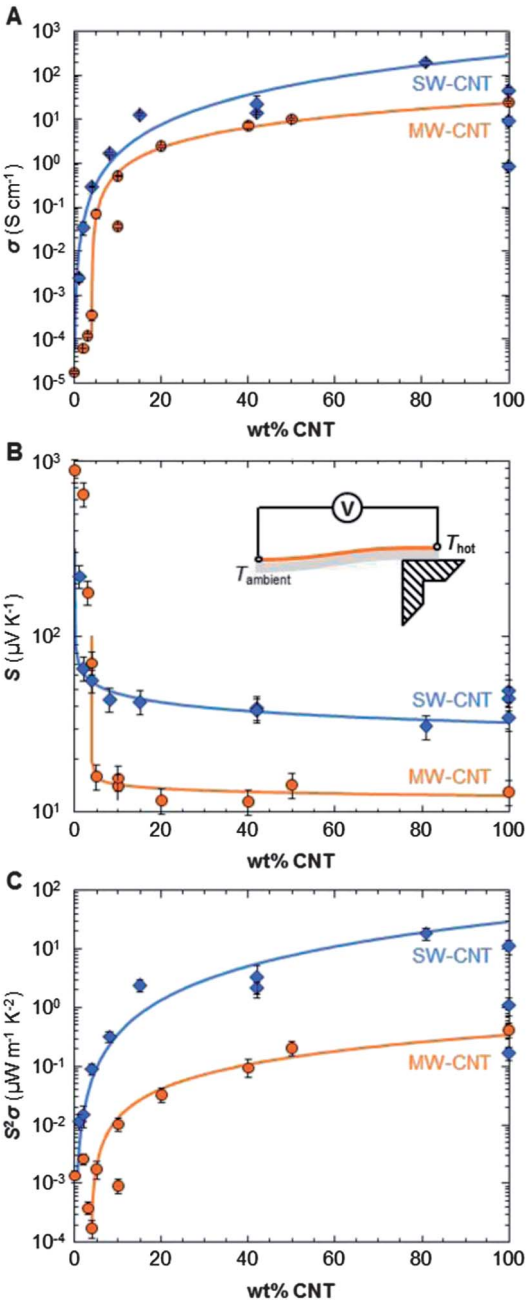

Fig. 2 Thermoelectric properties of pristine P3HT/CNT composites. (A) Electrical conductivity σ, (B) average Seebeck coefficient S and (C) power factor $S^2\sigma$ of P3HT/CNT blends based on MW-CNT (red circles) and SW-CNT (blue diamonds). Solid lines represent fits according to eqn (2) and (4). $S^2\sigma$ fits were produced by combining the fits of σ and S. Inset: schematic of the experimental setup used to measure S.

$p_{3D} = 2$ for a two- and three-dimensional network, respectively.[32] We find $p_{MW\text{-}CNT} \sim 1.3$ and $p_{SW\text{-}CNT} \sim 2.2$, which suggests a 2D MW-CNT and 3D SW-CNT network. This observation indicates that the former may display a certain degree of in-plane alignment whereas the latter feature little preferential orientation. In contrast, variable-angle spectroscopic ellipsometry (VASE) measurements revealed that the optical constants of both investigated P3HT/CNT composites are largely isotropic (ESI, Fig. S3†), which suggests that neither type of composites features a substantial degree of alignment. Thus, we conclude that the thermoelectric properties are unlikely to vary dramatically when comparing the in- and out-of-plane directions.

To further elucidate to which degree CNTs are distributed in the composite, scanning electron microscopy (SEM) was performed on a sample that contained 42 wt% SW-CNTs. The SEM image displayed in Fig. 3 reveals numerous flexible strands that are tightly embedded in a matrix. Their length is in excess of one micrometre and we measure an average diameter of 26 ± 2 nm, which is much larger than one nanometre, *i.e.* the typical diameter of single SW-CNTs. This observation indicates that SW-CNTs are present as small bundles, which are wrapped by P3HT molecules. Instead, for P3HT/MW-CNT composites we deduced a diameter of 38 ± 6 nm (ESI, Fig. S4†), which is only slightly larger than the average diameter of 10–15 nm of the used MW-CNTs. We propose that MW-CNTs are well-dispersed but again carry a P3HT mantle. Therefore, it can be expected that electrical conductance in the percolating network of the CNT bundles occurs due to tunnelling through the poorly conducting P3HT matrix rather than hopping, which requires direct electrical contact. We find that the following relation is obeyed above the percolation threshold, *i.e.* for $c > c^*$ (ESI, Fig. S5†):

$$\ln \sigma \propto c^{-1/3} \tag{3}$$

where c is the concentration of CNTs.[33] According to ref. 32, this correlation indicates that above the percolation threshold electrical transport is indeed limited by tunnel junctions.

We now turn to the dependence of the Seebeck coefficient with composition. First of all, we note that all samples displayed a positive value of the Seebeck coefficient, which is consistent with the p-type character of P3HT as well as CNTs. Below the percolation threshold, the Seebeck coefficient drops dramatically from the very high $S_{P3HT} \sim 878 \pm 132$ μV K^{-1} of reference P3HT as soon as CNTs are added (Fig. 2B). A much lower but constant value is reached at $c > c^*$, which appears to be equivalent to the value of reference CNT. A power law describes the variation of the Seebeck coefficient with CNT content reasonably well:

$$S = S_{CNT}|c - c^*|^p \tag{4}$$

where c is the CNT concentration and c^*, S_{CNT} and p are constants. c^* is the critical CNT concentration for percolation and we used the same values that we found when fitting the electrical conductivity with eqn (2). The pre-factor S_{CNT} is related to the intrinsic Seebeck coefficient of CNTs. We obtain $S_{MW\text{-}CNT} \sim 12$ μV K^{-1} and $S_{SW\text{-}CNT} \sim 32$ μV K^{-1}. The higher value of SW-CNTs is in accordance with their more semiconducting character. Furthermore, we observe that the change in Seebeck coefficient correlates with the percolation threshold. For $c \ll c^*$, CNTs are isolated and charge carriers have to cross large distances in the polymer matrix for electrical conduction to occur. Since the Seebeck coefficient depends on the electronic environment that charge carriers experience, we find $S_{P3HT} > S > S_{CNT}$. This is in contrast to the case $c > c^*$, in which $S \sim S_{CNT}$. This is because above the percolation threshold P3HT-coated CNT bundles are in sufficient proximity for tunnelling to occur and thus charge carriers predominately explore the more electrically conducting CNTs.

The overall performance of a thermoelectric material scales with the power factor. We observe that the power factor continues to improve with increasing CNT content for all compositions but SW-CNT reference films (Fig. 2C). For P3HT/MW-CNT composites a value of $S^2\sigma \sim 0.2 \pm 0.1$ μW m^{-1} K^{-2} is reached for $c_{MW\text{-}CNT} \sim 50$ wt% (neglecting reference MW-CNT), whereas P3HT/SW-CNT composites yield a two orders of magnitude higher $S^2\sigma \sim 18 \pm 4$ μW m^{-1} K^{-2} for $c_{SW\text{-}CNT} \sim 81$ wt%.

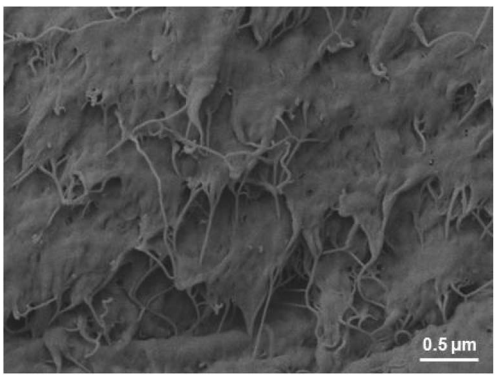

Fig. 3 Scanning electron micrograph of a cleaved film with $c_{SW\text{-}CNT} \sim 42$ wt%.

Thermal properties of undoped composites

An estimate of the figure of merit also requires knowledge of the thermal properties. Unfortunately, experimental limitations in our laboratories prevented us from conducting a full analysis of the thermal properties directly on films and over the full composition range. Instead, we investigated the thermal diffusivity α of one millimetre thick bulk samples that we had prepared by cold-pressing the dispersion-cast material. Together with measurements of the density ρ and specific heat capacity C_p, we could calculate the thermal conductivity according to:

$$\kappa = C_p \rho \alpha \tag{5}$$

We find that the investigated compositions of $c_{MW\text{-}CNT} \sim 10$ wt% and $c_{SW\text{-}CNT} \sim 8$ wt% show a value similar to that of the pure polymer (Table 1). Moreover, the thermal conductivity of reference P3HT $\kappa_{P3HT} \sim 0.19 \pm 0.05$ W m^{-1} K^{-1} agrees well with literature values.[20,34]

Table 1 Bulk thermal properties of P3HT/CNT composites: density ρ, specific heat capacity C_p at 25 °C, thermal diffusivity α and thermal conductivity κ

	ρ (g cm^{-3})	C_p (J g^{-1} K^{-1})	α (mm^2 s^{-1})	κ (W m^{-1} K^{-1})
P3HT	1.11 ± 0.01	1.84 ± 0.02	0.09 ± 0.01	0.19 ± 0.05
10 wt% MW-CNT	1.11 ± 0.01	1.43 ± 0.01	0.10 ± 0.03	0.16 ± 0.04
8 wt% SW-CNT	1.15 ± 0.01	1.44 ± 0.01	0.08 ± 0.02	0.13 ± 0.03

Despite the very high intrinsic thermal conductivity of single-walled carbon nanotubes $\kappa_{CNT} > 1000$ W m^{-1} K^{-1},[35] the thermal conductivity of P3HT/CNT composites remains low up to a filler content of at least $c_{MW\text{-}CNT} \sim 10$ wt% and $c_{SW\text{-}CNT} \sim 8$ wt%. This observation can be rationalised by considering the nature of thermal transport pathways in the composite, which comprises the P3HT matrix parallel to the CNT network. The CNT network is formed by CNTs in series with polymer-filled barriers. It has been argued that polymer material present at the CNT surface strongly impedes thermal transport by phonon-scattering but affects electrical transport to a much lesser extent.[12,17] This implies that the thermal conductance of CNTs is much higher than that of the polymer barrier. Thus, a simple parallel composite model suggests that the total thermal conductance is dominated by the thermal conductance of the polymer, which is consistent with the experimentally observed invariance in κ (*cf.* discussion in the ESI†). Intriguingly, it has been reported that thermoelectric composites of PEDOT:PSS with CNTs or Te nanorods display this type of behaviour, as evidenced by the fact that they retain the thermal properties of the polymer matrix up to a filler content of at least 60 and 80 wt%, respectively, when measured out-of-plane.[12,13] Certainly, addition of a much higher fraction of CNTs will eventually lead to a strong increase in thermal conductivity and therefore a full analysis ought to cover the full composition range and include in- and out-of-plane measurements. Thus, for the P3HT/CNT composites at hand we limit an estimate of the figure of merit to measured samples. We use the bulk thermal conductivities and assume an isotropic distribution of CNTs (*cf.* Fig. 3) to obtain a value of $ZT_{300K} \sim (2 \pm 1) \times 10^{-5}$ at $T = 300$ K for $c_{MW\text{-}CNT} \sim 10$ wt% and $ZT_{300K} \sim (7 \pm 2) \times 10^{-4}$ for $c_{SW\text{-}CNT} \sim 8$ wt%. However, we note that the power factor continues to increase with filler content and thus the maximum figure of merit that can be achieved with undoped P3HT/CNT composites is likely to be higher than the here reported values.

Doping of composites with $FeCl_3$

In as-cast composites electrical conduction predominantly occurs in the CNT phase. The surrounding P3HT is a semiconductor and acts as a spacer between adjacent CNTs that prevents good electrical contact. Thus, in a further series of experiments we studied the influence of p-doping of the polymer matrix. We used anhydrous $FeCl_3$ in nitromethane as the dopant. UV-vis spectroscopy of spin-coated thin films of reference P3HT as well as P3HT/CNT composites confirmed the dopant uptake by the polymer as evidenced by the rapid decrease in absorbance of neutral P3HT between 400 and 600 nm. This signal is separated by an isosbestic point from absorbance in the infrared, including one peak at 800 nm that appears upon doping due to bipolaron charge carriers (ESI, Fig. S7†).[8] The dopant concentration as well as doping time had a strong effect on the electrical properties (ESI, Fig. S8 and S9†). For a composite with $c_{MW\text{-}CNT} \sim 10$ wt% the electrical conductivity first strongly increased with dopant concentration and time but too high doping appeared to have a negative effect. This, we ascribe to the documented increase in brittleness with dopant uptake,[36] which may have introduced fractures during sample handling. Despite a maximum Seebeck coefficient at intermediate doping time the power factor continued to increase with further doping (ESI, Fig. S9†). Thus, we selected to work with doping parameters that offered a good compromise between brittleness and electrical performance, *i.e.* doping for one hour with 0.03 M anhydrous $FeCl_3$ in nitromethane.

Thermoelectric properties of doped composites

Having established optimum doping conditions, we next studied the influence of the CNT content on the electrical properties of doped composites. Doping of reference P3HT raised the electrical conductivity to $\sigma_{P3HT} \sim 8 \pm 2$ S cm^{-1}, whereas either type of CNTs appeared insensitive to the dopant. Irrespective of composition, doping significantly improved the electrical conductivity of all P3HT/CNT composites (Fig. 4A). This, we rationalise with the enhanced contribution of the polymer matrix to electrical conduction alongside the CNT network. Moreover, a pronounced increase in electrical conductivity at low CNT concentrations is followed by a decrease at high CNT concentrations in the case of P3HT/MW-CNT and a plateau for P3HT/SW-CNT composites, again accompanied by an underperforming SW-CNT reference. In contrast, the Seebeck coefficient appears to be independent of the CNT content with an average $\langle S \rangle \sim 29$ μV K^{-1} (Fig. 4B). Thus, also the power factor is maximised for intermediate compositions (Fig. 4C). This is most pronounced for P3HT/MW-CNT composites, which show an optimised $S^2\sigma \sim 6 \pm 2$ μW m^{-1} K^{-2} for $c_{MW\text{-}CNT} \sim 10$–40 wt%. In contrast, P3HT/SW-CNT composites yield a $S^2\sigma \sim 25 \pm 6$ μW m^{-1} K^{-2} for only $c_{SW\text{-}CNT} \sim 8$ wt% and a maximum $S^2\sigma \sim 95 \pm 12$ μW m^{-1} K^{-2} for $c_{SW\text{-}CNT} \sim$ 42–81 wt%.

According to several literature reports, the thermal conductivity of poly(3-alkylthiophene)s only weakly depends on the doping level and for highly doped P3HT a value of $\kappa_{P3HT} \sim 0.5$ W m^{-1} K^{-1} has been reported.[20,37,38] Our electrical conductivity measurements of reference CNT samples indicate that σ_{CNT} is little affected by exposure to $FeCl_3$. Thus, we use the literature value for highly doped P3HT to estimate a figure of merit $ZT_{300K} \sim 0.004 \pm 0.001$ for $c_{MW\text{-}CNT} \sim 10$ wt% and a $ZT_{300K} \sim 0.015 \pm 0.004$ for $c_{SW\text{-}CNT} \sim 8$ wt%. The power factor of P3HT/SW-CNT composites continues to increase with CNT content, which indicates that a $ZT_{300K} > 0.1$ is within reach with this type of material.

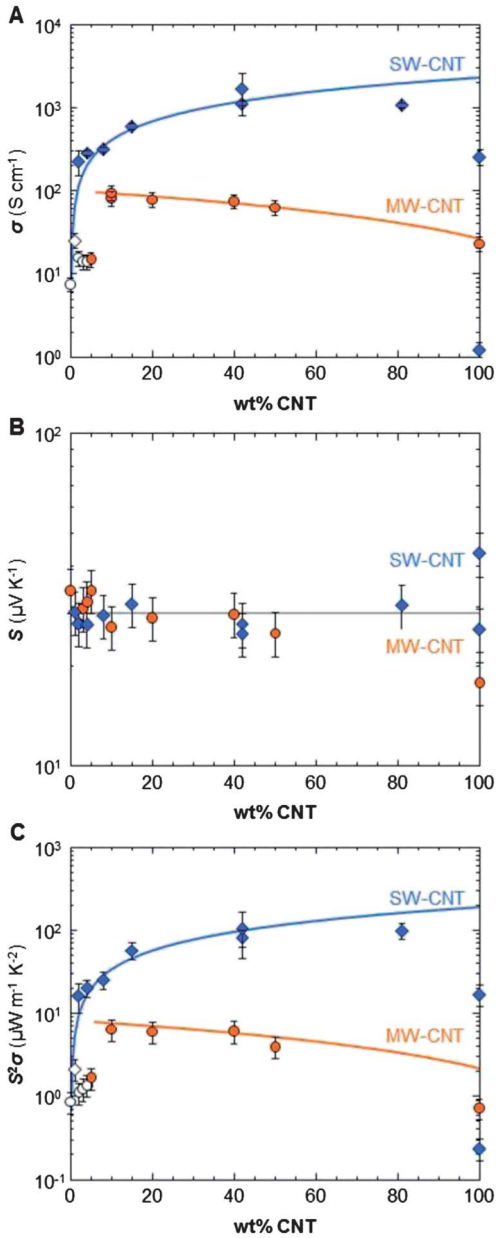

Fig. 4 Thermoelectric properties of $FeCl_3$-doped P3HT/CNT composites. (A) σ, (B) average S and (C) $S^2\sigma$ of composites based on MW-CNTs (red circles) and SW-CNTs (blue diamonds) that were doped for one hour with 0.03 M $FeCl_3$ in nitromethane. Solid lines represent fits: σ of P3HT/MW-CNT was fitted with a linear regression and σ of P3HT/SW-CNT was fitted with eqn (2); the average $\langle S \rangle$ of all doped samples excluding reference CNT was calculated; $S^2\sigma$ fits were produced by combining the fits of σ and S. Filled symbols: σ measured with the van der Pauw technique; open symbols: σ measured in 2-point configuration.

Stability of $FeCl_3$ doping

For practical applications, materials with long-term environmental stability are crucial. While $FeCl_3$-doping of P3HT is known to be unstable over long periods of time, especially at elevated temperatures $T > 80$ °C,[39] we found that the electrical conductivity only slowly decreased over the course of months (ESI, Fig. S10†). Composites with a high load of SW-CNT, *i.e.* $c_{SW\text{-}CNT} \sim 42$ wt%, showed an increased shelf-life with a promising half-life $\tau_{1/2} \sim 8$ months, whereas comparable MW-CNT based samples with $c_{MW\text{-}CNT} \sim 50$ wt% yielded only $\tau_{1/2} \sim 2$ months. Moreover, thermal cycling to 105 °C did not affect the electrical properties (ESI, Fig. S2†).

Conclusions

In summary, we have demonstrated that optimally p-doped composites of the conjugated polymer P3HT with a conducting filler material, *i.e.* carbon nanotubes, can display an encouraging thermoelectric performance. For P3HT/MW-CNT composites we estimate a maximum power factor $S^2\sigma \sim 6 \pm 2$ μW m^{-1} K^{-2} for a composition range of $c_{MW\text{-}CNT} \sim 10$–40 wt%. Instead, when using SW-CNTs we achieved a very promising $S^2\sigma \sim 95 \pm 12$ μW m^{-1} K^{-2} for $c_{SW\text{-}CNT} \sim 42$–81 wt%. Certainly, the here demonstrated electrical properties are significantly higher than those of either of the two constituents alone. Moreover, we could establish that the thermal conductivities of composites with a filler content of at least 10 wt% are comparable to $\kappa_{P3HT} \sim 0.19 \pm 0.05$ W m^{-1} K^{-1} of reference P3HT, which confirms the potential of this materials combination as a competitive p-type thermoelectric material.

Experimental

Materials

Regioregular P3HT (number- and weight-average molecular weight: $M_n \sim 30$ kg mol^{-1} and $M_w \sim 54$ kg mol^{-1}, regioregularity ~90%) and regiorandom P3HT were obtained from Rieke Metals (USA). Highly regioregular P3HT ($M_n \sim 32$ kg mol^{-1}, $M_w \sim 66$ kg mol^{-1}, regioregularity ~97%) was obtained from Ossila (UK).

HiPco SW-CNTs, high pressure carbon monoxide conversion, diameter ~ 0.7–1.3 nm, were purchased from Carbon Nanotechnologies Inc., TX, USA. The ratio of metallic to semiconducting CNTs is 1/3 to 2/3. Typically, contaminants such as the carbon-coated catalyst are present. MW-CNTs produced *via* catalytic CVD, diameter ~ 10–15 nm, all metallic, were purchased from Arkema France (purity >85%; a typical impurity is amorphous carbon).

Sample preparation

P3HT/CNT dispersions were prepared by first dispersing CNTs in *ortho*-dichlorobenzene (*o*DCB). Then, P3HT chloroform solution (5–20 g L^{-1}) was added and after each of a total of five addition steps the dispersion was mildly sonicated (sonicator model D80 from MRC; 33 kHz and 80 watt) for 100 min. The P3HT/CNT composition was varied by adding different absolute amounts of P3HT. Higher CNT contents were increasingly difficult to disperse and thus the total CNT concentration in *o*DCB was gradually reduced from 5 to 1 g L^{-1}. No surfactants were used for dispersion of CNTs. The homogeneity of dispersions was confirmed by visual inspection. Finally, the dispersion was cast on poly(ethylene terephthalate) (PET) foil to form 1–4 μm thick films. The thickness was measured with a P16+ surface profilometer from KLA Telcor. Bulk Samples for DSC, density and thermal diffusivity measurements were prepared by cold-pressing solidified material at a pressure of 15 kN cm^{-2}.

Samples were doped by submerging in anhydrous $FeCl_3$ nitromethane solutions followed by rinsing with ethanol to remove excess dopant.

Electrical characterisation

The electrical conductivity σ of square-shaped films was determined with the van der Pauw method[40] using an Ecopia HMS-3000 Hall measurement system. Where stated, σ was measured in two-point configuration.

The Seebeck coefficient S of films was characterised with a home-built setup under ambient atmosphere. A variable temperature gradient $\Delta T = T_{hot} - T_{ambient}$ was applied along approximately 10–20 mm long and 2–6 mm wide P3HT/CNT films on PET by tightly placing one end on a Kofler bench whilst keeping the other end at close to ambient temperature through suspension in air (*cf.* inset Fig. 1B). The temperature on either end was measured with thin film K-type thermocouples (Omega Engineering, UK) clamped to either end of the sample. Electrical contact with the samples was made with stainless steel clamps; in addition, for undoped samples silver paste was applied. A concealment provided protection from thermal convection and light. The potential difference ΔV was measured with a Keithley 2400 SourceMeter for ΔT ranging from 5 to 70 K. The average relative Seebeck coefficient $\Delta S = \Delta V/\Delta T = S - S_{steel}$ was estimated from the slope of a straight line fit to $\Delta V(\Delta T)$ (ESI, Fig. S11†). The absolute average Seebeck coefficient S of the sample was estimated by taking into account the average Seebeck coefficient of stainless steel $S_{steel} \sim -1.4$ μV K^{-1}.[41]

The temperature dependence of S and σ was measured with a Linseis LSR-3 system. Within the experimental error, the values obtained using both setups are in good agreement.

Thermal characterisation

The thermal conductivity of bulk samples was obtained from the equation $\kappa = C_p \rho \alpha$, where C_p is the specific heat capacity, ρ the density and α the thermal diffusivity. DSC was performed under nitrogen at a scan rate of 10 °C min^{-1} with a Mettler Toledo TA8000/DSC820 instrument to obtain C_p. The floatation technique in water/sodium chloride was used to estimate ρ. A home-built setup was used to measure α under steady state conditions; thermal convection was avoided by placing the setup in mild vacuum of 0.1 mbar. One millimetre thick bulk samples were sandwiched between gold-coated copper blocks, which acted as the heat source and sink, respectively. Good thermal contact was ensured by adding a layer of molten gallium between samples and copper blocks.

UV-vis absorbance spectroscopy

UV-vis spectra of P3HT/CNT thin films spin-coated on glass were recorded with a Varian Cary 5000 spectrophotometer.

Variable-angle spectroscopic ellipsometry (VASE)

VASE was performed with a SOPRALAB rotating polariser ellipsometer (GES-5E) coupled to a CCD detector.

Scanning electron microscopy (SEM)

SEM was performed with a JEOL JSM-7400F instrument. Pristine samples were imaged, *i.e. no* gold coating was used.

Acknowledgements

This work was supported by the Ministerio de Economía y Competitividad through Grant CSD2010-00044 (Consolider NANOTHERM). C.M. gratefully acknowledges financial support from the CSIC through the JAE-Doc program (European Social Fund). M.C.-Q. thanks the Ministerio de Economía y Competitividad for funding through a Ramón y Cajal fellowship. M.S.M.-G. acknowledges the ERC for funding through an ERC 2008 Starting Grant "Nano-TEC" number 240497. R.Y.-R. holds the Stanley D. and Nikki Waxberg professorial chair in Advanced Materials. Finally, we would like to thank Camilla Lindqvist (Chalmers) for proficient help with SEM imaging on short notice.

References

1 G. J. Snyder, *Electrochem. Soc. Interface*, 2008, **17**(3), 54–56.
2 T. J. Seebeck, *Abhandlungen der Königlichen Preußischen Akademie der Wissenschaften zu Berlin*, 1825, **1822–1823**, 265–273.
3 The Seebeck coefficient $S = \Delta V/\Delta T$ provides a measure for the potential difference ΔV that is generated across a material as long as its ends are exposed to a temperature difference ΔT.
4 J. P. Fleurial, L. Gailliard and R. Triboulet, *J. Phys. Chem. Solids*, 1988, **49**, 1237–1247.
5 T. O. Poehler and H. E. Katz, *Energy Environ. Sci.*, 2012, **5**, 8110–8115.
6 O. Bubnova and X. Crispin, *Energy Environ. Sci.*, 2012, **5**, 9345–9362.
7 Y. W. Park, *Synth. Met.*, 1991, **45**, 173–182.
8 Y. Xuan, X. Liu, S. Desbief, P. Leclère, M. Fahlman, R. Lazzaroni, M. Berggren, J. Cornil, D. Emin and X. Crispin, *Phys. Rev. B: Condens. Matter Mater. Phys.*, 2010, **82**, 115454.
9 Y. Shinohara, K. Ohara, H. Nakanishi, Y. Imai and Y. Isoda, *Mater. Sci. Forum*, 2005, **492–493**, 141–144.
10 O. Bubnova, Z. U. Khan, A. Malti, S. Braun, M. Fahlman, M. Berggren and X. Crispin, *Nat. Mater.*, 2011, **10**, 429–433.
11 O. Bubnova, M. Berggren and X. Crispin, *J. Am. Chem. Soc.*, 2012, **134**, 16456–16459.
12 K. C. See, J. P. Feser, C. E. Chen, A. Majumdar, J. J. Urban and R. A. Segalman, *Nano Lett.*, 2010, **10**, 4664–4667.
13 C. Yu, K. Choi, L. Yin and J. C. Grunlan, *ACS Nano*, 2011, **5**, 7885–7892.
14 Y. Sun, P. Sheng, C. Di, F. Jiao, W. Xu, D. Qiu and D. Zhu, *Adv. Mater.*, 2012, **24**, 932–937.
15 Q. Zhang, Y. Sun, W. Xu and D. Zhu, *Energy Environ. Sci.*, 2012, **5**, 9639–9644.
16 R. B. Äich, N. Blouin, A. Bouchard and M. Leclerc, *Chem. Mater.*, 2009, **21**, 751–757.
17 Q. Yao, L. Chen, W. Zhang, S. Liufu and X. Chen, *ACS Nano*, 2010, **4**, 2445–2451.

18 C. Meng, C. Liu and S. Fan, *Adv. Mater.*, 2010, **22**, 535–539.
19 Y. Du, S. Z. Shen, W. D. Yang, K. F. Cai and P. S. Casey, *Synth. Met.*, 2012, **162**, 375–380.
20 M. He, J. Ge, Z. Lin, X. Feng, X. Wang, H. Lu, Y. Yang and F. Qiu, *Energy Environ. Sci.*, 2012, **5**, 8351–8358.
21 C. Yu, Y. S. Kim, D. Kim and J. C. Grunlan, *Nano Lett.*, 2008, **8**, 4428–4432.
22 Y. S. Kim, D. Kim, K. J. Martin, C. Yu and J. C. Grunlan, *Macromol. Mater. Eng.*, 2010, **295**, 431–436.
23 C. A. Hewitt, A. B. Kaiser, S. Roth, M. Craps, R. Czerw and D. L. Caroll, *Appl. Phys. Lett.*, 2011, **98**, 183110.
24 Y. Choi, Y. Kim, S.-G. Park, Y.-G. Kim, B.-J. Sung, S.-Y. Jang and W. Kim, *Org. Electron.*, 2011, **12**, 2120–2125.
25 A. Ikeda, K. Nobusawa, T. Hamano and J. Kikuchi, *Org. Lett.*, 2006, **8**, 5489–5492.
26 J. Geng, B.-S. Kong, S. B. Yang, S. C. Youn, S. Park, T. Joo and H.-T. Jung, *Adv. Funct. Mater.*, 2008, **18**, 2659–2665.
27 J. Liu, J. Zou and L. Zhai, *Macromol. Rapid Commun.*, 2009, **30**, 1387–1391.
28 M. Bernardi, M. Giulianini and J. C. Grossman, *ACS Nano*, 2010, **4**, 6599–6606.
29 O. Inganäs, W. R. Salaneck, J.-E. Österholm and J. Laakso, *Synth. Met.*, 1988, **22**, 395–406.
30 W. Bauhofer and J. Z. Kovacs, *Compos. Sci. Technol.*, 2009, **69**, 1486–1498.
31 J. N. Coleman, S. Curran, A. B. Dalton, A. P. Davey, B. McCarthy, W. Blau and R. C. Barklie, *Phys. Rev. B: Condens. Matter Mater. Phys.*, 1998, **58**, R7492–R7495.
32 E. Kymakis and G. A. J. Amaratunga, *J. Appl. Phys.*, 2006, **99**, 084302.
33 Note that the observed trend in σ can also be understood in terms of a parallel composite model, which suggests for $c \ll c^*$ a value close to σ_{P3HT} whereas for $c \gg c^*$ a linear trend is predicted (*cf.* discussion in the ESI and Fig. S6†).
34 J. A. Malen, K. Baheti, T. Tong, Y. Zhao, J. A. Hudgings and A. Majumdar, *J. Heat Transfer*, 2011, **133**, 081601.
35 C. Yu, L. Shi, Z. Yao, D. Li and A. Majumdar, *Nano Lett.*, 2005, **5**, 1842–1846.
36 J. Moulton and P. Smith, *Synth. Met.*, 1991, **40**, 13–22.
37 B.-Y. Lu, C.-C. Liu, S. Lu, J.-K. Xu, F.-X. Jiang, Y.-Z. Li and Z. Zhang, *Chin. Phys. Lett.*, 2010, **27**, 057201.
38 J. Sun, M.-L. Yeh, B. J. Jung, B. Zhang, J. Feser, A. Majumdar and H. E. Katz, *Macromolecules*, 2010, **43**, 2897–2903.
39 Y. Wang and M. F. Rubner, *Synth. Met.*, 1990, **39**, 153–175.
40 L. J. Van der Pauw, *Philips Tech. Rev.*, 1958, **20**, 220–224.
41 R. S. Graves, T. G. Kollie, D. L. McElroy and K. E. Gilchrist, *Int. J. Thermophys.*, 1991, **12**, 409–415.